MIND: Material Interface Generation from UDFs for Non-Manifold Surface Reconstruction

Xuhui Chen[1,2], **Fei Hou**[1,2,*], **Wencheng Wang**[1,2,*], **Hong Qin**[3], **Ying He**[4]
[1]Key Laboratory of System Software (CAS) and State Key Laboratory of Computer Science, Institute of Software, Chinese Academy of Sciences
[2]University of Chinese Academy of Sciences
[3]Department of Computer Science, Stony Brook University
[4]College of Computing and Data Science, Nanyang Technological University
{chenxh, houfei, whn}@ios.ac.cn qin@cs.stonybrook.edu yhe@ntu.edu.sg

Abstract

Unsigned distance fields (UDFs) are widely used in 3D deep learning due to their ability to represent shapes with arbitrary topology. While prior work has largely focused on learning UDFs from point clouds or multi-view images, extracting meshes from UDFs remains challenging, as the learned fields rarely attain exact zero distances. A common workaround is to reconstruct signed distance fields (SDFs) locally from UDFs to enable surface extraction via Marching Cubes. However, this often introduces topological artifacts such as holes or spurious components. Moreover, local SDFs are inherently incapable of representing non-manifold geometry, leading to complete failure in such cases. To address this gap, we propose MIND (Material Interface from Non-manifold Distance fields), a novel algorithm for generating material interfaces directly from UDFs, enabling non-manifold mesh extraction from a global perspective. The core of our method lies in deriving a meaningful spatial partitioning from the UDF, where the target surface emerges as the interface between distinct regions. We begin by computing a two-signed local field to distinguish the two sides of manifold patches, and then extend this to a multi-labeled global field capable of separating all sides of a non-manifold structure. By combining this multi-labeled field with the input UDF, we construct material interfaces that support non-manifold mesh extraction via a multi-labeled Marching Cubes algorithm. Extensive experiments on UDFs generated from diverse data sources, including point cloud reconstruction, multi-view reconstruction, and medial axis transforms, demonstrate that our approach robustly handles complex non-manifold surfaces and significantly outperforms existing methods. The source code is available at https://github.com/jjjkkyz/MIND.

1 Introduction

Signed Distance Fields (SDFs) are a widely adopted implicit representation for watertight surfaces due to their simplicity and effectiveness. The sign in SDFs clearly distinguishes the inside and outside of a surface, enabling straightforward surface extraction via well-established methods such as Marching Cubes (MC) [1]. While recent adaptations of SDF [2–5] incorporate constraints to support open surface reconstruction, they remain inadequate for capturing non-manifold structures.

Unsigned Distance Fields (UDFs), in contrast, eliminate the need for sign information and provide a more flexible framework capable of representing a wide range of surface topologies, including

*Corresponding authors.

39th Conference on Neural Information Processing Systems (NeurIPS 2025).

open and closed surfaces, non-manifold geometries, and shapes with complex internal structures [6–19]. However, this flexibility comes at a significant cost: the absence of sign information makes it significantly harder to identify zero-level sets, especially in the presence of non-manifold structures.

Several methods have been proposed for surface extraction from UDFs. A common strategy involves reconstructing local SDFs from UDFs using gradient-based estimation [6, 11, 20] or neural prediction [21] to approximate sign information and identify zero-level set intersections. While these methods benefit from the efficiency of Marching Cubes, they are highly sensitive to UDF inaccuracies, often resulting in holes and redundant components. Other approaches [22, 23] generalize dual contouring [24] to improve reconstruction quality, but they often introduce unintended non-manifold artifacts due to inconsistent topological handling. Mesh deformation methods, such as DCUDF [25, 26], improve robustness by iteratively shrinking an initial double-layered manifold surface to fit the target geometry. However, since the initial surface is always manifold and the deformation process preserves this structure, these methods are inherently incapable of capturing non-manifold geometries. Mesh extraction algorithms based on Dual Contouring [24] have the ability to extract non-manifold structures, but they also generate a large number of non-manifold faces in manifold regions. To our knowledge, there is currently no method that can effectively extract the correct non-manifold structures from UDFs.

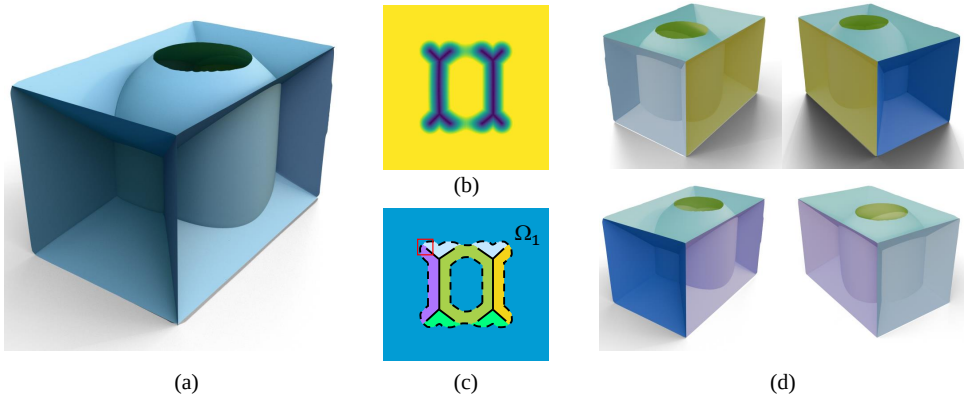

Figure 1: An open non-manifold surface (a) with 7 sides, including the top, bottom, left, right, front, back, and inner regions. Given the input unsigned distance field (A cross section is illustrated in (b)), we generate the corresponding material interface (c). For supporting open surfaces, we generate an envelope Ω_1 (the dashed lines in (c)) enclosing the surface. To generate MI partitions, it needs to fill the gaps, e.g., the gap within the red box in (c), between Ω_1 and the surface boundaries. We extend the surface boundaries slightly to intersect with Ω_1. The redundant faces are removed while extracting the surface by M3C [27]. The reconstructed mesh in shown in four views (d) where each side is highlighted in a different color for clarity.

On the other hand, non-manifold structures are ubiquitous in many applications, such as anatomical modeling [28, 29], composite materials [30, 31], multi-phase fluids [32–35], and bubble simulations [36, 37]. These structures are characterized by complex topologies and often arise as interfaces between multiple materials, commonly referred to as **material interfaces** (MIs) [38]. An MI defines a partitioning of the spatial domain into multiple labeled regions $\{F_1, ..., F_n\}$ as shown in Figure 1(c).

Traditional MI representations are limited to closed surfaces, i.e., surfaces without boundaries. As illustrated in Figure 1, we define an enclosing envelope Ω_1 around the surface. The surface boundaries are extended slightly to intersect with Ω_1 to form MI partitions inside Ω_1. The outside of Ω_1 is treated as background and assigned the label F_0. This generalization allows us to deal with not only closed but also certain open non-manifold surfaces and to apply multi-label Marching Cubes methods, such as M3C [27], to reconstruct non-manifold meshes from such labeled partitions. Redundant surfaces, such as faces adjacent to the background, are removed.

However, MI is not a universal representation, as it requires predefined partition domain information. In practical applications, MIs are typically defined by known functions (e.g., from fluid simulations) or derived based on numerical priors (e.g., from CT images). In contrast, UDFs serve as a more universal

representation and have been widely adopted in many classic 3D reconstruction tasks, such as point cloud reconstruction [6–12], multi-view image reconstruction [13–16] and 3D generation [17–19].

To address these limitations, we introduce a novel algorithm to generate MIs from the input UDFs without requiring predefined partition domain information, which enables accurate non-manifold surface extraction from MIs.

Our method consists of three key steps. First, we generate a two-labeled field to distinguish between the two sides of a local surface patch using positive and negative signs. Second, we extend the local two-signed field into a global multi-labeled field, assigning unique labels to each side of a non-manifold surface. The multi-labeled field is then combined with the input UDF to generate the target MI. Third, we refine the extracted mesh from the MI to ensure both visual accuracy and topological coherence. We evaluate our method on a variety of datasets and UDF learning methods. Experimental results demonstrate that our approach generates clean meshes that accurately capture non-manifold structures, where existing methods often fail.

The main contributions of the paper are as follows:

1. We develop an algorithm for generating MIs from learned UDFs, enabling robust non-manifold surface reconstruction without requiring prior knowledge of MIs. By extending the definition of the MI, Our approach effectively handles both closed models and open models.
2. We introduce a novel algorithm that extends the local two-sided field—capable of distinguishing the two sides of local manifold patches—into a global multi-labeled field, enabling the differentiation of multiple sides of non-manifold surfaces.
3. We conduct extensive evaluations across diverse datasets and UDF learning methods. Experimental results demonstrate the capability of our method in extracting clean and accurate manifold and non-manifold meshes, outperforming existing techniques.

2 Related Works

2.1 Manifold Reconstruction

Recently, deep learning approaches have gained traction in surface reconstruction. These methods learn SDFs [39–49] or occupancy fields [50, 51] using neural networks directly from point clouds or multi-view images. These methods typically extract surfaces from signed distance fields [1, 52], which inherently guarantee watertight manifold models. Extensions of SDFs to support open surfaces typically involve introducing additional constraints or masks [2–5]. While these methods offer greater adaptability and flexibility in modeling, they remain fundamentally restricted to manifold surfaces.

2.2 Non-manifold Reconstructions

Unsigned distance fields have emerged as a promising alternative for representing surfaces with diverse topologies, including open surfaces, non-manifold geometries, and shapes with complex internal structures [6–11, 13–19, 53]. By discarding the sign term of SDFs, UDFs offer greater flexibility, enabling the representation of complex models, including non-manifold surfaces. However, most UDF-based methods primarily focus on open manifold surfaces, with limited exploration of non-manifold surface reconstruction. The primary obstacle lies in the lack of a robust mesh extraction algorithm tailored for non-manifold structures from UDFs.

Recent advancements have focused on extracting the zero-level sets from UDFs using modified Marching Cubes. Some methods [6, 11, 20, 21] reconstruct local sign information to determine edge intersections. DCUDF [25] refines the mesh of non-zero level sets to approximate the zero-level set through shrinking, producing double-layered results. However, these methods fail to effectively handle non-manifold geometries.

For non-manifold structures, sampling point clouds from UDFs and applying non-manifold-specific methods [54] have been explored but suffer from low accuracy and robustness. Dual Contouring-based methods, such as NDC [22] and DMUDF [23], have the potential to generate non-manifold geometries but either lack generalizability or introduce unintended non-manifold artifacts. Manifold DC [55] avoids such artifacts but cannot model non-manifold structures.

Existing non-manifold mesh extraction algorithms are predominantly applied in the context of material interfaces (MIs). MI represents a collection of regions where the target surface corresponds to the intersection of different regions. MI is widely utilized in partitioned domains, such as anatomical structures [28, 29], composite materials [30, 31], bubbles [36, 37], and multi-phase fluids [32–35], where space is naturally segmented into distinct regions.Using the MI as input, multi-label algorithms, such as M3C [27], handle non-manifold surfaces by leveraging explicit material interface definitions. While effective, they require predefined region labels or arrangements, limiting their applicability.

In this paper, we aim to address the limitations of these approaches by introducing a novel method for generating MIs directly from UDFs. Unlike previous methods, our approach does not require prior knowledge of material interfaces or region labels, enabling the robust extraction of non-manifold surfaces directly from UDFs.

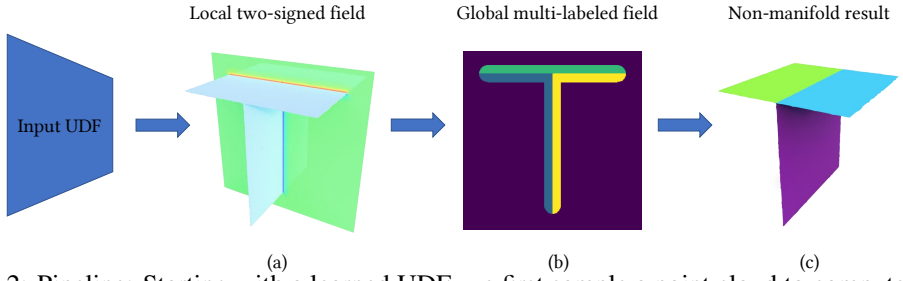

Figure 2: Pipeline: Starting with a learned UDF, we first sample a point cloud to compute a local two-signed field to differentiate the two sides of local manifold patches (a). We do not calculate regions far from the target face and label them as background (the green region in (a)). This is followed by generating a global multi-labeled field based on the two-signed field, which distinguishes all sides of the non-manifold surface (b). Finally, the non-manifold surface is extracted from the multi-labeled distance field using a multi-label MC algorithm (c).

3 Method

In this work, we generate MIs from input UDFs to enable the extraction of non-manifold meshes from UDFs. As illustrated in Figure 2, our method consists of three key steps: In Section 3.1, we construct a local two-signed field to distinguish the two sides of manifold patches within the input UDF. In Section 3.2, the local two-signed field is extended to a global multi-labeled field to capture the sides of non-manifold surfaces, forming the target MI. Finally, in Section 3.3, we describe how to extract non-manifold surface meshes from the MI.

3.1 Local Two-Signed Fields

To generate the MI of the input UDF, we need to segment the 3D space into different partitions. As shown in Figure 2, our first step is to generate a two-signed local side field that distinguishes the two sides of local manifold patches. Similar to the generalized winding number [56, 57], on a surface S, given consistently oriented normals $\mathbf{n_x}$ of points $\mathbf{x} \in S$, we introduce the following indicator function $w_S^l(\mathbf{q})$ to compute a side field for a query point $\mathbf{q}$:

$$w_S^l(\mathbf{q}) = \int_{\mathbf{x}\in\mathcal{N}_S(\mathbf{q})} \frac{(\mathbf{x}-\mathbf{q})\cdot\mathbf{n_x}}{\|\mathbf{x}-\mathbf{q}\|^3+\epsilon} d\mathbf{x}, \tag{1}$$

where ϵ is a small positive to avoid division by zero. Different from the generalized winding number, the region of integration is modified from the entire surface S to a local neighborhood $\mathcal{N}_S(\mathbf{q})$ on S around the point $\mathbf{q}$. This adjustment allows w_S^l to distinguish between the two sides of a local manifold using positive and negative signs.

Implementation Details We extract a point cloud from the given UDF. Points are sampled randomly in space Ω_1 where the UDF values are equal to a threshold r_1 and these points are projected toward local minima, similar to the approach in [10]. The point cloud is then downsampled using uniform grid voxels to obtain a uniform initial point cloud $\mathcal{P}$. Next, we apply [58] to compute oriented

normals for the points. Although [58] may result in flipped normals, the orientations are piecewise consistent, ensuring that most are oriented consistently. The discrete form of $w_S^l(\mathbf{q})$ is,

$$w_S^l(\mathbf{q}) = \sum_{\mathbf{x}_i \in \mathcal{N}_\mathcal{P}(\mathbf{q})} \frac{(\mathbf{x}_i - \mathbf{q}) \cdot \mathbf{n}_i}{\|\mathbf{x}_i - \mathbf{q}\|^3 + \epsilon}. \tag{2}$$

We discretize the space into voxels and compute the side field only for the voxels o_i inside Ω_1, as points far from the surface are not of interest. Any voxel outside Ω_1 is considered background and assigned the label F_0. $w_S^l(\mathbf{q})$ is locally defined and is able to distinguish the two sides where the normals are properly defined. In particular, in regions near non-manifold edges or regions with flipped normals, w_S^l is not well-defined. These issues will be refined in the following Section 3.2.

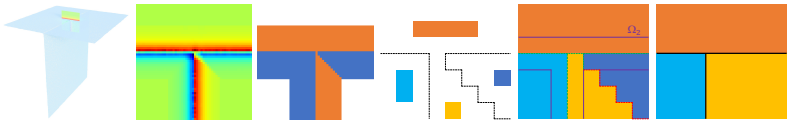

(a) (b) (c) (d) (e)

Figure 3: Illustration of global multi-labeled field generation from the local two-signed field on a T-shaped model. The close-up view of the cross-section on the non-manifold structure is provided. The local two-signed field w_S^l is first computed (a). Applying connected component labeling to the local two-signed field introduces artifacts due to small "tubes" (b). Erosion effectively removes these connected "tubes" (c). We solve the Equation 3 to fill the blank region (d). Comparing to dilate operation, it produce a more consistent boundary to the origin labeling (dash line). But our current result is over-segmented. We introduce an envelope Ω_2 that is closer to the target surface than Ω_1. As shown in (e), the partition boundaries inside Ω_2 is shown in green and outside in red. We merge two regions whose most adjacent boundaries are in red to get the final labeling result (e).

3.2 Global Multi-Labeled Fields

In this section, we generate the global multi-labeled distance field, which is able to distinguish all sides of a non-manifold surface, from the local two-signed side field. We cluster voxels based on the two signs of w_S^l by applying the 3D connected component labeling algorithm[2]. This algorithm assigns a label F_i to each voxel that is connected and has the same sign (positive or negative). As a result, voxels within Ω_1 are split into a set of partitions $\{R_k\}$. However, non-manifold or normal flipping regions, where three or more partitions coincide, are scarcely possible to be properly divided only by the two signs of w_S^l. As shown in Figure 3, a partition may span across non-manifold edges via a narrow "tube". Since this tube is thin, a simple morphological erosion can remove it, causing the remaining voxels of the partition to become disconnected.

We denote the eroded voxels by R_k^e and the remaining voxels by R_k^r. For the voxels in all the connected components of R_k^r, we assign different new labels F_k to different connected components of R_k^r. Each voxel in R_k^e should be labeled by one of the labels of F_k. The goal is to minimize variations in neighboring labels of R_k^e. Therefore, we minimize the following energy for labeling:

$$\begin{aligned}
&\min_f \sum_{o_i \in \cup_k R_k^e} D\left(f(o_i)\right) + \sum_{(o_i,o_j)\in\mathcal{N}} V\left(f(o_i), f(o_j)\right), \\
&s.t.\ f(o_i) = f_s(o_i),\ o_i \in \cup_k R_k^r \\
&D\left(f(o_i)\right) = \begin{cases} 0, & \text{if } f(o_i) \in F_k \text{ or } F_k = \Phi \\ 1, & \text{otherwise} \end{cases}, \quad (o_i \in R_k^e) \\
&V\left(f(o_i), f(o_j)\right) = \begin{cases} 0, & \text{if } f(o_i) = f(o_j) \\ 1, & \text{otherwise} \end{cases}
\end{aligned} \tag{3}$$

Here, $f(o_i)$ represents the to be solved label assigned to voxel o_i, $f_s(o_i)$ denotes the label assigned to voxels in R_k^r, which are fixed, and $\mathcal{N}$ refers to the set of neighboring voxels. The function $V(\cdot)$ minimizes label changes, while $D(\cdot)$ ensures that most of the interfaces between partitions remain

[2] `https://github.com/seung-lab/connected-components-3d`

invariant. Occasionally, R_k may be so small that R_k^r and F_k are empty sets. In such cases, we omit the constraint. Equation (3) can be solved using α-expansion [59].

After refinement, the partitions ensure that the two sides of a non-manifold belong to different partitions. However, over-segmented partitions may exist, as shown in Figure 3, which are unavoidable in the two-signed field near non-manifold edges. These over-partitions should be merged. Otherwise they would lead to redundant surfaces in the reconstructed mesh. Two partitions that are not separated by the surface S should be merged. Directly assessing this condition can be tricky, so instead, we construct another envelope, Ω_2, by extracting an iso-surface at value r_2 ($r_2 < r_1$) from the UDF. This gives us the relation $S \subset \Omega_2 \subset \Omega_1$. If two partitions are separated by S, their boundary voxels should lie within Ω_2. Conversely, if two partitions are not separated by S, most of their boundary voxels should be outside Ω_2, but still within $\Omega_1 - \Omega_2$. As illustrated in Figure 3, through these simple tests, we can effectively merge redundant partitions, ensuring that different sides of a non-manifold surface belong to different partitions, and no further merging of partitions is needed. These partition labels along with the input UDF constitute the target MI.

3.3 Non-Manifold Surface Extraction

With the target MI, we can extract the non-manifold mesh $\mathcal{M}$ using a multi-label Marching Cubes algorithm. Specifically, we adopt the M3C method [27] with minor modifications. Instead of interpolating at the midpoint of each cube edge, we use the value of w_S^l to determine the intersection points, enhancing accuracy. We do not generate the face associated with the background label F_0 because there is no target surface at the interface between the background and other regions, which also enables open model reconstruction. To further refine the mesh, redundant triangular faces extending from surface boundaries outside Ω_2 are removed.

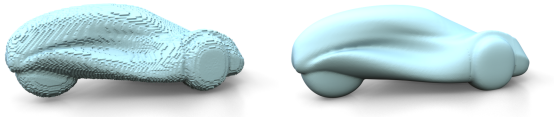

(a) (b)

Figure 4: The Multi-Labeled Field computed from the point cloud, while having the correct topology, generates a noisy mesh because its zero level set is misaligned with the target surface (a). We use the input UDF to refine the result (b).

However, the accuracy of w_S^l remains limited by discretization. To address this limitation, we refine the extracted mesh $\mathcal{M}$ by optimizing its alignment with the input UDF as shown in Figure 4. Inspired by DCUDF [25], we fine-tune $\mathcal{M}$ by minimizing its UDF values for improved accuracy while incorporating a Laplacian regularization term to maintain the mesh's shape and prevent face folding. Unlike DCUDF, our mesh $\mathcal{M}$ contains non-manifold edges, where traditional Laplacian computation is not well-defined. For a point $\mathbf{p}_m$ on a non-manifold edge, using all adjacent points to compute the Laplacian fails to prevent face folding, as illustrated in Figure 5. To overcome this, we group adjacent triangular faces based on the labels they border. Every triangular face belongs to two groups. Each group of triangular faces forms a manifold mesh. For a point $\mathbf{p}_i \in \mathcal{M}$, the Laplacians are computed separately in each group of adjacent faces. For example, for a point on the non-manifold edge of a T-shape, there are 3 groups of adjacent faces and 3 Laplacian terms. We optimize the following loss function to refine the mesh,

$$\min_{\pi} \sum_{s \in \mathcal{S}} \Big(\sum_{\mathbf{p}_i \in \mathcal{M}^s} f(\pi(\mathbf{p}_i)) + \lambda_1 \sum_{\mathbf{p}_i \in \mathcal{M}^s} \Big\| \pi(\mathbf{p}_i) - \frac{1}{|\mathcal{N}^s(\mathbf{p}_i)|} \sum_{\mathbf{p}_j \in \mathcal{N}^s(\mathbf{p}_i)} \pi(\mathbf{p}_j) \Big\|^2 \Big), \tag{4}$$

where $f(\cdot)$ denotes the UDF values and $\pi(\mathbf{p}_i)$ is the new location of point $\mathbf{p}_i$ after optimization. $\mathcal{S}$ denotes the set of signs and $\mathcal{M}^s$ is the sub-mesh whose faces border on the sign s. $\mathcal{N}^s(\mathbf{p}_i)$ denotes the 1-ring neighboring points of $\mathbf{p}_i$ in $\mathcal{M}^s$. The first term, $f(\pi_1(\mathbf{p}_i))$, drives the points $\mathbf{p}_i$ toward the local minima of the UDF. The second Laplacian term prevents the triangular face from folding.

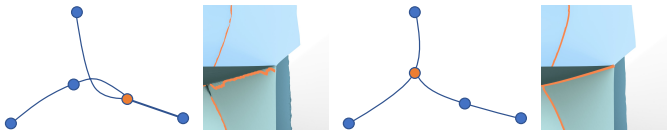

(a) (b) (c) (d)

Figure 5: Laplacian constraint of non-manifold edges. For a point (orange) on a non-manifold edge, traditional Laplacian constraint fails to prevent adjacent faces from folding. By computing the Laplacian loss within each labeled region separately, our method effectively avoids self-intersections of the surface.

4 Experimental Results

4.1 Experimental Setup and Hyperparameters

We normalize 3D models to fit within $[-0.5, 0.5]^3$ and use a bounding box of $[-0.6, 0.6]^3$ to contain the UDFs. For calculating the local two-signed field, we sample 1 million points on the r_1 level set and optimize their positions to align with the local minima of the UDF. The resolution is set to 256^3, resulting in a voxel size of 0.0046. The voxel size for point cloud downsampling[3] is set to 0.005, which is slightly higher than 0.0046. While the downsampled point cloud has a density of 0.005, we set $r_2 = 0.01$ to generate a continuous Ω_2. To ensure Ω_1 is larger than Ω_2, r_1 is set to 0.05. We erode the local two-signed field 2 times before generating the global multi-labeled field. Two partitions in the global multi-labeled field are merged if the number of boundary voxels within $\Omega_1 - \Omega_2$ is three times greater than the number of voxels within Ω_2. A more detailed experiment of hyperparameters can be found in Section A of appendix.

We use M3C [27] to extract meshes, implemented in Dream3D[4]. We then optimize the output of M3C with Equation 4 for 200 iterations, using a Laplacian weight of 1000, to generate the final result. Although several hyperparameters are introduced in our paper, most of them correspond to the resolution and exhibit generalizability across different types of learned distance fields. All results are tested on a single NVIDIA V100 GPU.

4.2 Comparisons

Baselines To the best of our knowledge, no prior work investigates generating MIs from UDFs. Since the extracted meshes depend on MI qualities, we compare our method against two unsupervised UDFs mesh extraction algorithms, including DCUDF [25], and DMUDF [23]. While DCUDF uses double-layered manifold meshes to approximate non-manifold structures, DMUDF is capable of generating non-manifold edges. To assess the topological correctness of the extracted meshes, we compute geodesic distances, which are highly sensitive to topological features. Specifically, we use the heat method [60] with a non-manifold Laplacian [61] applied to the extracted meshes. For comparison, geodesic distances are also computed on dense points, serving as a reference.

UDFs Learned from Point Clouds We learn UDFs from unoriented point clouds using CAPUDF [6], LevelSetUDF [7], and DEUDF [8], respectively. The results are shown in Figure 6, with non-manifold edges highlighted in red. We compare our method with DMUDF and DCUDF.

DMUDF [23], a Dual Contouring variant, is capable of generating non-manifold edges. However, the process of generating non-manifolds in DC is often uncontrolled, resulting in a significant number of non-manifold edges appearing in regions that should remain manifold. Furthermore, DMUDF utilizes an octree structure to accelerate the algorithm. To determine whether the target surface exists within a specific leaf node, DMUDF relies on a key criterion based on the UDF value at the node's center point. This approach is highly sensitive to UDF accuracy, making it prone to failure in the presence of noise or inaccuracies in the UDF. Such issues can cause the octree subdivision process to terminate prematurely. As highlighted in DUDF [9], most UDF learning methods prioritize accurate distance predictions near the target surface but neglect accuracy in regions farther away. This limitation can

[3] `https://www.open3d.org`

[4] `https://github.com/BlueQuartzSoftware/DREAM3D`

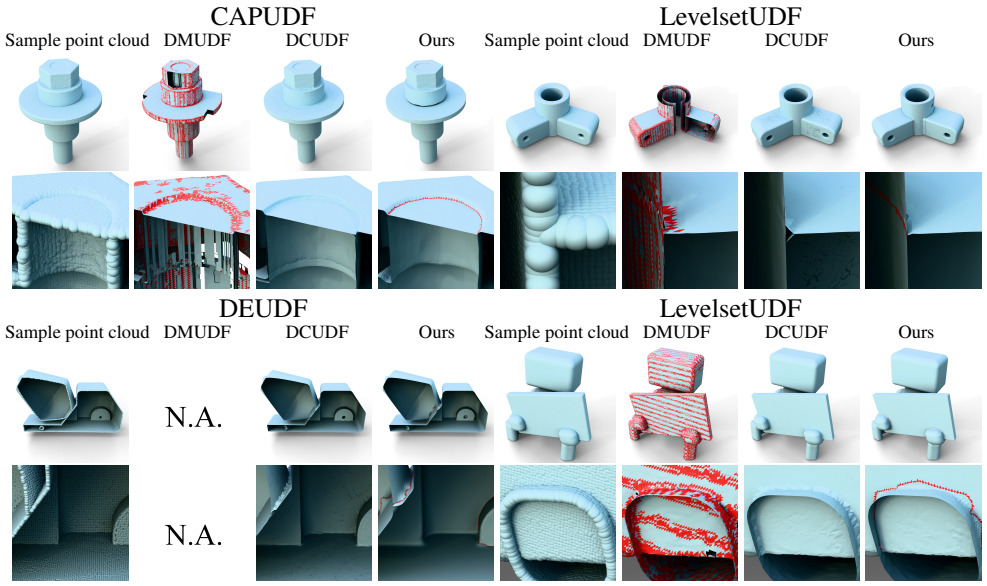

Figure 6: Non-manifold surface extraction from UDFs learned by CAPUDF [6], LevelSetUDF [7], and DEUDF [8]. We present the sampled point cloud on the UDFs as the GT (Ground Truth). We compare our surface extraction method with DCUDF and DMUDF, highlighting non-manifold edges in red in the results. While DMUDF frequently produces non-manifold edges in regions that should be manifold, DCUDF consistently generates double-layered manifold meshes, leading to a failure in preserving the correct topology of the target surfaces.

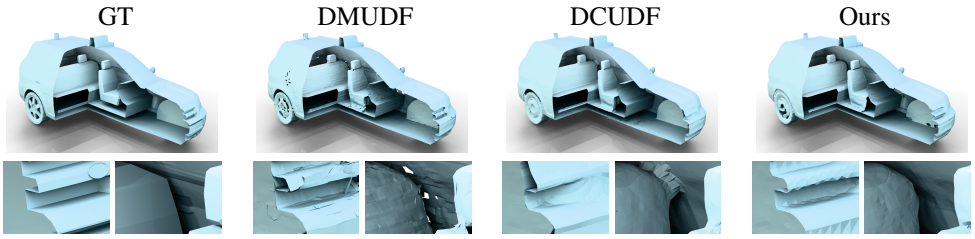

Figure 7: Surface extraction from UDFs learned by CAPUDF [6] on the ShapeNet-Car dataset [62].

result in significant missing regions in DMUDF's output when a node's center point is far from the vicinity of the target surface. DCUDF [25] approximates the target non-manifold surfaces using a double-layer mesh. Although the results visually align with the target surface, the lack of exact coincidence between the two layers often introduces undesired artifacts, such as redundant shadows, during rendering.

To assess the quality of the extracted meshes, we sample 100K points on the mesh and employ the Chamfer distance L2 as a geometrical metric. Table 1 presents the results on the ShapeNet-Car [62] dataset and DeepFashion3D [63] dataset. The visualization results of ShapeNet-Car dataset are shown in Figure 7, where our visual results are the best.

Table 1: Evaluation on the ShapeNet-Car [62] dataset learned from CAP-UDF[6] and DeepFashion3D dataset [63] learned from DCUDF[25].

Dataset	DMUDF			DCUDF			Ours		
	Mean	Median	Std	Mean	Median	Std	Mean	Median	Std
ShapeNet-Car	3.086	2.564	2.112	3.290	2.770	2.252	2.917	2.447	2.107
DeepFashion3D	1.792	1.383	0.512	1.825	1.495	0.535	1.770	1.339	0.507

UDFs Learned from Multi-view Images Extracting surfaces from UDFs learned via multi-view images presents significant challenges, especially in scenes involving transparent objects or thin structures, where non-manifold surfaces are prevalent.

We evaluate our method and compare it with baselines on UDFs generated by NU-NeRF [43] on multi-view images of transparent objects. NU-NeRF learns two separate SDFs, corresponding to the outer and inner objects, and extracts their respective meshes using Marching Cubes. To prevent the inner SDF from producing meshes in the outer region, NU-NeRF uses the outer SDF as a mask during extraction. However, this masking approach often leads to redundant components forming along the mask boundaries. Although NU-NeRF employs a post-processing step to remove these redundant components, it creates discontinuities between the inner and outer meshes.

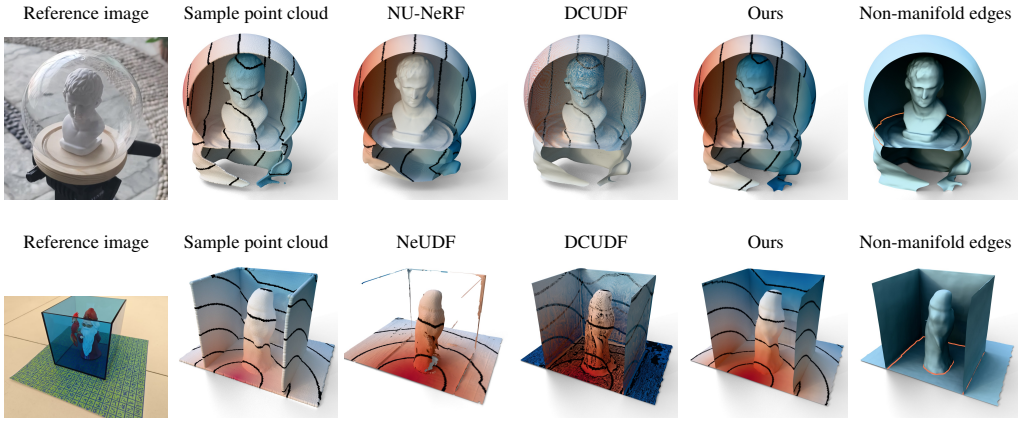

Figure 8: Non-manifold surface extraction from UDFs learned by NU-NeRF [43] (top) and NeUDF [15] (bottom). Geodesic distances computed on the extracted meshes are visualized to validate their non-manifold topology. The geodesic distances computed on sampled point clouds are used as reference for comparison. All baseline methods fail to accurately preserve the non-manifold structures in the extracted meshes.

To address this, we combine the two SDFs[5] to a single UDF for mesh extraction. The outer SDF value is directly applied in the outer region, while for the inner region, we use the minimum absolute value of the two SDFs. As shown in Figure 8, adopting the geodesic distance measure, we confirm that our results preserve the correct topology. For comparison, we also use DCUDF to extract the target surface. While DCUDF produces visually pleasing results, its double-layered structure prevents geodesic distances from diffusing between layers, highlighting its limitation in preserving topological consistency.

We also adopt NeUDF [15] for learning UDFs from multi-view images of transparent objects. The results are presented in Figure 8. NeUDF employs MeshUDF [20], a gradient-based Marching Cubes, for mesh extraction from learned UDFs. However, this approach fails in non-manifold regions due to the lack of a suitable lookup table for non-manifolds in standard Marching Cubes. Furthermore, unlike opaque objects whose boundary surfaces align with zero-level sets, transparent objects typically exhibit iso-values that are not close to zero, leading to complete reconstruction failure for transparent objects. DCUDF addresses this limitation by extracting non-zero level sets, allowing it to capture transparent objects. However, its double-layered mesh structure significantly compromises topological accuracy. In contrast, our method successfully reconstructs transparent objects and accurately models their non-manifold surfaces. This highlights the robustness and versatility of our approach compared to existing methods.

UDFs Induced from Q-MDF [64] Non-manifold structures frequently appear in medial axes. Q-MDF [64] computes medial axes for watertight models through the joint learning of signed distance fields and medial fields (MF) [65]. It has been shown that the difference between the SDF and MF yields an unsigned distance field [64]. In the original Q-MDF pipeline, medial axes are extracted using DCUDF [25], which, as mentioned above, generates a double-layered manifold mesh. Consequently,

[5]We use the SDFs provided directly by the NU-NeRF authors.

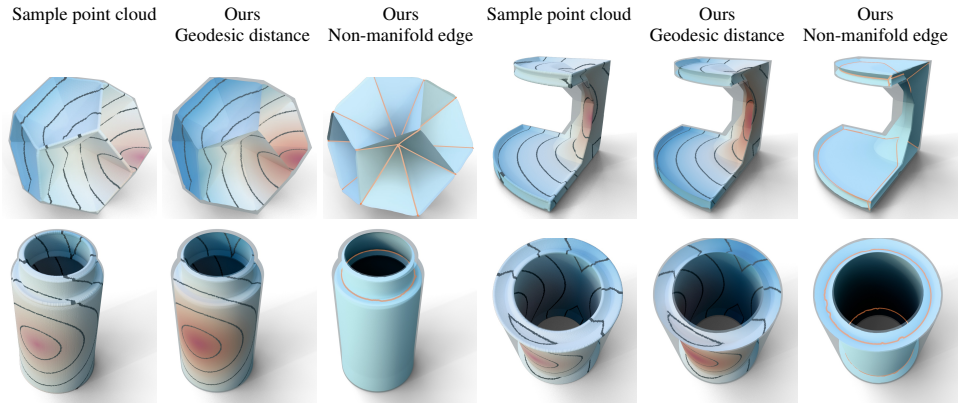

Figure 9: Non-manifold surface extraction from UDFs learned by Q-MDF [64]. The target surfaces are medial axes, characterized by numerous non-manifold structures. For clarity, we render both the watertight surfaces and their corresponding medial axes. Geodesic distances are computed on the extracted non-manifold medial axes and compared with those on the sampled point clouds for validation.

this approach fails to preserve the non-manifold characteristics of medial axes. By utilizing MIND, we extract high-quality, single-layered non-manifold medial axes, as demonstrated in Figure 9.

Limitations We use α-expansion [59] to label voxel grids, which is time-consuming. The primary bottleneck arises from evaluating all potential label distributions across the entire voxel grid for each candidate label. A feasible acceleration strategy involves partitioning the voxel grid into blocks, where block-wise α-expansion computation effectively reduces costs. Another alternative is to use dilation instead of alpha expansion, which has a time cost independent of the number of labels but yields an approximate solution. On the other hand, our approach requires an erosion operation, which may inadvertently remove small or thin MI regions and lead to missing facets, as shown in Figure 10.

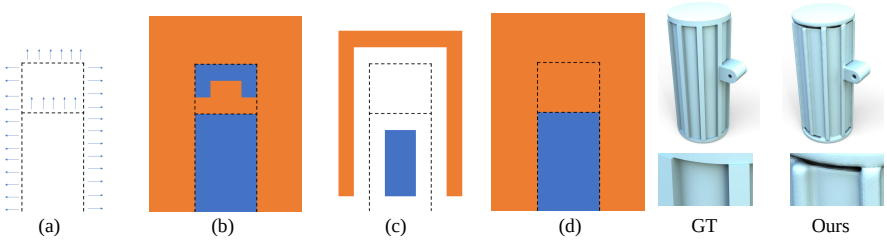

Figure 10: For a small MI region (upper part) (a), the inner voxels of its local two-signed field (b) will be removed during the erosion process, resulting in no seed region in the entire internal space (c). Consequently, the structure cannot be recovered after α-expansion (d).

5 Conclusions

In this paper, we introduce MIND, a novel algorithm to extract MIs from UDFs for non-manifold mesh extraction. By combining the strengths of material interfaces and unsigned distance fields, MIND supports non-manifold reconstruction from UDFs. MIND does not require pre-defined partition information, making it suitable for a broader range of scenarios. Our experimental results across various types of UDFs demonstrate the effectiveness of MIND in generating MIs for accurate non-manifold mesh reconstruction. In its current form, our implementation generates MI from pre-learned UDFs, making the presented method primarily a zero-level set extraction algorithm. It is highly desired to develop techniques that learn an MI directly from raw input data, such as point clouds or multi-view images. Such advancements could significantly broaden the range of applications for MI and enhance its utility in tackling complex reconstruction tasks.

Acknowledgments and Disclosure of Funding

This project was partially supported by the National Key R&D Program of China (2023YFB3002901), the Research Projects of ISCAS (ISCAS-JCMS-202303, ISCAS-ZD-202401, ISCAS-JCZD-202402, ISCAS-JCMS-202403), and the Ministry of Education, Singapore, under its Academic Research Fund Grant (RT19/22).

References

[1] William E. Lorensen and Harvey E. Cline. Marching cubes: A high resolution 3d surface construction algorithm. In *Proc. of ACM SIGGRAPH*, pages 163–169, 1987.

[2] Li Wang, Yu-Tao Liu, Jie Yang, Weikai Chen, Xiaoxu Meng, Bo Yang, Jintao Li, and Lin Gao. Hsdf: Hybrid sign and distance field for neural representation of surfaces with arbitrary topologies. *IEEE Transactions on Visualization and Computer Graphics*, pages 1–14, 2024.

[3] Xiaoxu Meng, Weikai Chen, and Bo Yang. Neat: Learning neural implicit surfaces with arbitrary topologies from multi-view images. In *Proc. of CVPR*, pages 248–258, 2023.

[4] Zhen Liu, Yao Feng, Yuliang Xiu, Weiyang Liu, Liam Paull, Michael J. Black, and Bernhard Schölkopf. Ghost on the shell: An expressive representation of general 3d shapes. In *The Twelfth International Conference on Learning Representations*, 2024.

[5] Weikai Chen, Cheng Lin, Weiyang Li, and Bo Yang. 3psdf: Three-pole signed distance function for learning surfaces with arbitrary topologies. In *Proc. of CVPR*, pages 18501–18510, 2022.

[6] Junsheng Zhou, Baorui Ma, Yu-Shen Liu, Yi Fang, and Zhizhong Han. Learning consistency-aware unsigned distance functions progressively from raw point clouds. In *Advances in Neural Information Processing Systems (NeurIPS)*, 2022.

[7] Junsheng Zhou, Baorui Ma, Shujuan Li, Yu-Shen Liu, and Zhizhong Han. Learning a more continuous zero level set in unsigned distance fields through level set projection. In *Proc. of ICCV*, pages 3158–3169, 2023.

[8] Cheng Xu, Fei Hou, Wencheng Wang, Hong Qin, Zhebin Zhang, and Ying He. Details enhancement in unsigned distance field learning for high-fidelity 3D surface reconstruction. In *Proc. of AAAI*, pages 8806–8814, 2025.

[9] Miguel Fainstein, Viviana Siless, and Emmanuel Iarussi. Dudf: Differentiable unsigned distance fields with hyperbolic scaling. In *Proceedings of the IEEE/CVF Conference on Computer Vision and Pattern Recognition (CVPR)*, pages 4484–4493, June 2024.

[10] Julian Chibane, Aymen Mir, and Gerard Pons-Moll. Neural unsigned distance fields for implicit function learning. In *Advances in Neural Information Processing Systems (NeurIPS)*, December 2020.

[11] Siyu Ren, Junhui Hou, Xiaodong Chen, Ying He, and Wenping Wang. GeoUDF: Surface reconstruction from 3d point clouds via geometry-guided distance representation. In *Proc. of ICCV*, pages 14214–14224, 2023.

[12] Jiangbei Hu, Yanggeng Li, Fei Hou, Junhui Hou, Zhebin Zhang, Shengfa Wang, Na Lei, and Ying He. A lightweight UDF learning framework for 3D reconstruction based on local shape functions. In *IEEE/CVF Conference on Computer Vision and Pattern Recognition, CVPR 2025*, pages 1297–1307, 2025.

[13] Junkai Deng, Fei Hou, Xuhui Chen, Wencheng Wang, and Ying He. 2S-UDF: A Novel Two-stage UDF Learning Method for Robust Non-watertight Model Reconstruction from Multi-view Images. In *2024 IEEE/CVF Conference on Computer Vision and Pattern Recognition (CVPR)*, pages 5084–5093, 2024.

[14] Xiaoxiao Long, Cheng Lin, Lingjie Liu, Yuan Liu, Peng Wang, Christian Theobalt, Taku Komura, and Wenping Wang. Neuraludf: Learning unsigned distance fields for multi-view reconstruction of surfaces with arbitrary topologies. In *Proc. of CVPR*, pages 20834–20843, 2023.

[15] Yu-Tao Liu, Li Wang, Jie Yang, Weikai Chen, Xiaoxu Meng, Bo Yang, and Lin Gao. Neudf: Learning neural unsigned distance fields with volume rendering. In *Proc. of CVPR*, pages 237–247, 2023.

[16] Wenyuan Zhang, Kanle Shi, Yu-Shen Liu, and Zhizhong Han. Learning unsigned distance functions from multi-view images with volume rendering priors. In *European Conference on Computer Vision*, pages 397–415. Springer, 2024.

[17] Junsheng Zhou, Weiqi Zhang, Baorui Ma, Kanle Shi, Yu-Shen Liu, and Zhizhong Han. Udiff: Generating conditional unsigned distance fields with optimal wavelet diffusion. In *Proceedings of the IEEE/CVF Conference on Computer Vision and Pattern Recognition*, 2024.

[18] Yu-Tao Liu, Xuan Gao, Weikai Chen, Jie Yang, Xiaoxu Meng, Bo Yang, and Lin Gao. Dreamudf: Generating unsigned distance fields from a single image. *ACM Trans. Graph.*, 43(6), November 2024.

[19] Longwen Zhang, Ziyu Wang, Qixuan Zhang, Qiwei Qiu, Anqi Pang, Haoran Jiang, Wei Yang, Lan Xu, and Jingyi Yu. Clay: A controllable large-scale generative model for creating high-quality 3d assets. *ACM Trans. Graph.*, 43(4), July 2024.

[20] Benoit Guillard, Federico Stella, and Pascal Fua. Meshudf: Fast and differentiable meshing of unsigned distance field networks. In *European Conference on Computer Vision*, 2022.

[21] Federico Stella, Nicolas Talabot, Hieu Le, and Pascal Fua. Neural surface detection for unsigned distance fields. In *European Conference on Computer Vision*, pages 394–409. Springer, 2024. ISBN 978-3-031-73636-0.

[22] Zhiqin Chen, Andrea Tagliasacchi, Thomas Funkhouser, and Hao Zhang. Neural dual contouring. *ACM Transactions on Graphics (Special Issue of SIGGRAPH)*, 41(4), 2022.

[23] Congyi Zhang, Guying Lin, Lei Yang, Xin Li, Taku Komura, Scott Schaefer, John Keyser, and Wenping Wang. Surface extraction from neural unsigned distance fields. *2023 IEEE/CVF International Conference on Computer Vision (ICCV)*, pages 22474–22483, 2023.

[24] Tao Ju, Frank Losasso, Scott Schaefer, and Joe Warren. Dual contouring of hermite data. *ACM Trans. Graph.*, 21(3):339–346, 2002.

[25] Fei Hou, Xuhui Chen, Wencheng Wang, Hong Qin, and Ying He. Robust zero level-set extraction from unsigned distance fields based on double covering. *ACM Trans. Graph.*, 42(6), dec 2023.

[26] Xuhui Chen, Fugang Yu, Fei Hou, Wencheng Wang, Zhebin Zhang, and Ying He. DCUDF2: Improving efficiency and accuracy in extracting zero level sets from unsigned distance fields. *IEEE Transactions on Visualization and Computer Graphics*, 31:9052 – 9065, 2025.

[27] Ziji Wu and John M. Sullivan Jr. Multiple material marching cubes algorithm. *International Journal for Numerical Methods in Engineering*, 58(2):189–207, 2003.

[28] Martin Bertram, Gerd Reis, Rolf H. van Lengen, Sascha Köhn, and Hans Hagen. Non-manifold Mesh Extraction from Time-varying Segmented Volumes used for Modeling a Human Heart. In Ken Brodlie, David Duke, and Ken Joy, editors, *EUROVIS 2005: Eurographics / IEEE VGTC Symposium on Visualization*. The Eurographics Association, 2005.

[29] Yongjie Zhang, Thomas J.R. Hughes, and Chandrajit L. Bajaj. An automatic 3d mesh generation method for domains with multiple materials. *Computer Methods in Applied Mechanics and Engineering*, 199(5):405–415, 2010. Computational Geometry and Analysis.

[30] Scott Dillard, John Bingert, Dan Thoma, and Bernd Hamann. Construction of simplified boundary surfaces from serial-sectioned metal micrographs. *IEEE Transactions on Visualization and Computer Graphics*, 13(6):1528–1535, November 2007.

[31] M. Haitham Shammaa, Yutaka Ohtake, and Hiromasa Suzuki. Segmentation of multi-material ct data of mechanical parts for extracting boundary surfaces. *Comput. Aided Des.*, 42:118–128, 2010.

[32] Xiaosheng Li, Xiaowei He, Xuehui Liu, Baoquan Liu, and Enhua Wu. Multiphase surface tracking with explicit contouring. In *Proceedings of the 20th ACM Symposium on Virtual Reality Software and Technology*, VRST '14, page 31–40, New York, NY, USA, 2014. Association for Computing Machinery.

[33] Robert I. Saye and James A. Sethian. The voronoi implicit interface method for computing multiphase physics. *Proceedings of the National Academy of Sciences*, 108(49):19498–19503, 2011.

[34] Byungmoon Kim. Multi-phase fluid simulations using regional level sets. *ACM Trans. Graph.*, 29(6), December 2010.

[35] Frank Losasso, Tamar Shinar, Andrew Selle, and Ronald Fedkiw. Multiple interacting liquids. *ACM Trans. Graph.*, 25(3):812–819, July 2006. ISSN 0730–0301.

[36] Peter Heiss-Synak, Aleksei Kalinov, Malina Strugaru, Arian Etemadi, Huidong Yang, and Chris Wojtan. Multi-material mesh-based surface tracking with implicit topology changes. *ACM Trans. Graph.*, 43(4), July 2024.

[37] Wen Zheng, Jun-Hai Yong, and Jean-Claude Paul. Simulation of bubbles. *Graphical Models*, 71 (6):229–239, 2009. 2006 ACM SIGGRAPH/Eurographics Symposium on Computer Animation (SCA 2006).

[38] Xingyi Du, Qingnan Zhou, Nathan Carr, and Tao Ju. Robust computation of implicit surface networks for piecewise linear functions. *ACM Trans. Graph.*, 41(4), July 2022.

[39] Peng Wang, Lingjie Liu, Yuan Liu, Christian Theobalt, Taku Komura, and Wenping Wang. Neus: Learning neural implicit surfaces by volume rendering for multi-view reconstruction. *NeurIPS*, 2021.

[40] Yiqun Wang, Ivan Skorokhodov, and Peter Wonka. HF-NeuS: Improved Surface Reconstruction Using High-Frequency Details. In S. Koyejo, S. Mohamed, A. Agarwal, D. Belgrave, K. Cho, and A. Oh, editors, *Advances in Neural Information Processing Systems*, volume 35, pages 1966–1978. Curran Associates, Inc., 2022.

[41] Qiancheng Fu, Qingshan Xu, Yew Soon Ong, and Wenbing Tao. Geo-Neus: Geometry-Consistent Neural Implicit Surfaces Learning for Multi-view Reconstruction. In S. Koyejo, S. Mohamed, A. Agarwal, D. Belgrave, K. Cho, and A. Oh, editors, *Advances in Neural Information Processing Systems*, volume 35, pages 3403–3416. Curran Associates, Inc., 2022.

[42] Lior Yariv, Yoni Kasten, Dror Moran, Meirav Galun, Matan Atzmon, Basri Ronen, and Yaron Lipman. Multiview Neural Surface Reconstruction by Disentangling Geometry and Appearance. In H. Larochelle, M. Ranzato, R. Hadsell, M.F. Balcan, and H. Lin, editors, *Advances in Neural Information Processing Systems*, volume 33, pages 2492–2502. Curran Associates, Inc., 2020.

[43] Jia-Mu Sun, Tong Wu, Ling-Qi Yan, and Lin Gao. Nu-nerf: Neural reconstruction of nested transparent objects with uncontrolled capture environment. *ACM Trans. Graph.*, 43(6), November 2024. ISSN 0730-0301.

[44] Jeong Joon Park, Peter Florence, Julian Straub, Richard Newcombe, and Steven Lovegrove. Deepsdf: Learning continuous signed distance functions for shape representation. In *Proc. of CVPR*, pages 165–174, 2019.

[45] Baorui Ma, Zhizhong Han, Yu-Shen Liu, and Matthias Zwicker. Neural-pull: Learning signed distance function from point clouds by learning to pull space onto surface. In *ICML*, volume 139, pages 7246–7257, 2021.

[46] Baorui Ma, Junsheng Zhou, Yu-Shen Liu, and Zhizhong Han. Towards better gradient consistency for neural signed distance functions via level set alignment. In *2023 IEEE/CVF Conference on Computer Vision and Pattern Recognition (CVPR)*, pages 17724–17734, 2023.

[47] Yifan Wang, Lukas Rahmann, and Olga Sorkine-Hornung. Geometry-consistent neural shape representation with implicit displacement fields. In *Proc. of ICLR*, 2022.

[48] Alexandre Boulch and Renaud Marlet. Poco: Point convolution for surface reconstruction. In *Proceedings of the IEEE/CVF Conference on Computer Vision and Pattern Recognition (CVPR)*, pages 6302–6314, June 2022.

[49] Matan Atzmon and Yaron Lipman. Sal: Sign agnostic learning of shapes from raw data. In *IEEE/CVF Conference on Computer Vision and Pattern Recognition (CVPR)*, June 2020.

[50] Lars Mescheder, Michael Oechsle, Michael Niemeyer, Sebastian Nowozin, and Andreas Geiger. Occupancy networks: Learning 3d reconstruction in function space. In *Proc. of CVPR*, pages 4455–4465, 2019.

[51] Amine Ouasfi and Adnane Boukhayma. Unsupervised occupancy learning from sparse point cloud. In *2024 IEEE/CVF Conference on Computer Vision and Pattern Recognition (CVPR)*, pages 21729–21739, 2024.

[52] Silvia Sellán, Christopher Batty, and Oded Stein. Reach for the spheres: Tangency-aware surface reconstruction of sdfs. In *SIGGRAPH Asia 2023 Conference Papers*, SA '23, New York, NY, USA, 2023. Association for Computing Machinery.

[53] Jiayi Kong, Chen Zong, Junkai Deng, Xuhui Chen, Fei Hou, Shiqing Xin, Junhui Hou, Chen Qian, and Ying He. Voronoi-assisted diffusion for computing unsigned distance fields from unoriented points. *ArXiv*, abs/2510.12524, 2025.

[54] Jianning Wang, Manuel M. Oliveira, and Arie E. Kaufman. Reconstructing manifold and non-manifold surfaces from point clouds. In *Proc. of IEEE Visualization*, pages 415–422, 2005.

[55] Scott Schaefer, Tao Ju, and Joe Warren. Manifold dual contouring. *IEEE Transactions on Visualization and Computer Graphics*, 13(3):610–619, 2007.

[56] Alec Jacobson, Ladislav Kavan, and Olga Sorkine-Hornung. Robust inside-outside segmentation using generalized winding numbers. *ACM Trans. Graph.*, 32(4), July 2013. ISSN 0730-0301.

[57] Gavin Barill, Neil G. Dickson, Ryan Schmidt, David I. W. Levin, and Alec Jacobson. Fast winding numbers for soups and clouds. *ACM Trans. Graph.*, 37(4), July 2018. ISSN 0730-0301.

[58] Hugues Hoppe, Tony DeRose, Tom Duchamp, John McDonald, and Werner Stuetzle. Surface reconstruction from unorganized points. In *Proc. of ACM SIGGRAPH*, SIGGRAPH '92, pages 71–78, New York, NY, USA, 1992.

[59] Yuri Boykov, Olga Veksler, and Ramin Zabih. Fast approximate energy minimization via graph cuts. *IEEE Transactions on Pattern Analysis and Machine Intelligence*, 23(11):1222–1239, 2001.

[60] Keenan Crane, Clarisse Weischedel, and Max Wardetzky. The heat method for distance computation. *Communications of the ACM*, 60(11):90–99, 2017.

[61] Nicholas Sharp and Keenan Crane. A laplacian for nonmanifold triangle meshes. *Computer Graphics Forum*, 39(5):69–80, 2020.

[62] Angel X. Chang, Thomas Funkhouser, Leonidas Guibas, Pat Hanrahan, Qixing Huang, Zimo Li, Silvio Savarese, Manolis Savva, Shuran Song, Hao Su, Jianxiong Xiao, Li Yi, and Fisher Yu. Shapenet: An information-rich 3d model repository, 2015.

[63] Heming Zhu, Yu Cao, Hang Jin, Weikai Chen, Dong Du, Zhangye Wang, Shuguang Cui, and Xiaoguang Han. Deep fashion3d: A dataset and benchmark for 3d garment reconstruction from single images. In *Proc. of ECCV*, pages 512–530, 2020.

[64] Jiayi Kong, Chen Zong, Jun Luo, Shiqing Xin, Fei Hou, Hanqing Jiang, Chen Qian, and Ying He. Quasi-medial distance field (Q-MDF): A robust method for approximating and discretizing neural medial axis. *ArXiv*, abs/2410.17774, 2024.

[65] Daniel Rebain, Ke Li, Vincent Sitzmann, Soroosh Yazdani, Kwang Moo Yi, and Andrea Tagliasacchi. Deep medial fields. *CoRR*, 2021.

A Hyper-parameter study

In our pipeline, we use a resolution-dependent voxel size to downsample the point cloud. As Figure 11 shows, a smaller voxel size does not affect the result but introduces a larger computational overhead. Conversely, if the voxel size is set too large (e.g., 0.01), the point cloud becomes too sparse and holes appear in the reconstructed model. Our r_1 and r_2 values are also set according to the resolution to maintain them within proper ranges. As shown in Figure 12, moderate changes in these parameters are acceptable, but excessive adjustments can cause problems. Though a large r_1 does not introduce issues beyond computational overhead, an overly small r_1 (e.g., 0.03) could cause the erosion step to delete all regions, leading to reconstruction failure. An excessively large r_2 (e.g., 0.02) can lead to insufficient region merging, whereas an overly small r_2 (e.g., 0.0025) can result in unnecessary merging.

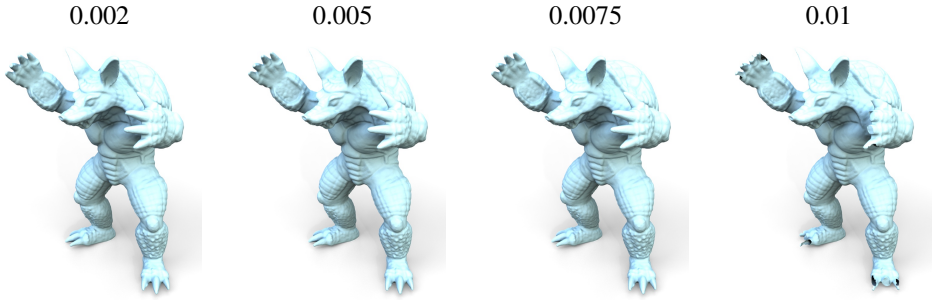

Figure 11: The reconstruction results with different downsampling voxel size.

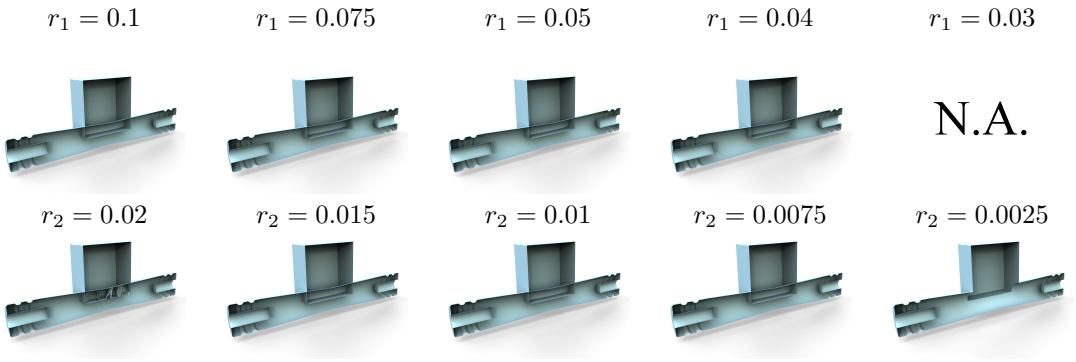

Figure 12: Mesh reconstruction with different r_1 and r_2. N.A. means reconstruction failed.

B More Results

We present additional results in the appendix, including point cloud reconstruction, multi-view reconstruction, and medial axis transforms. As illustrated in Figure. 13, our method can model real-world non-manifold structures defined by multi-view images, such as intersections between transparent objects and overlapping thin plate structures. These configurations represent challenging cases for signed distance fields to represent in practical scenarios. For point cloud reconstruction and medial axis transformations, we present additional results in Figure. 14 and Figure. 15, demonstrating the versatility of our approach. We also collected some more complex data to further illustrate the robustness of our method, as shown in Figure 16.

C Failed Case

As illustrated in Figure 17, the two sides of the non-orientable surface are indistinguishable, resulting in the absence of a well-defined MI. Consequently, our method fails to generate MIs for the surface, leading to artifacts in the extracted mesh.

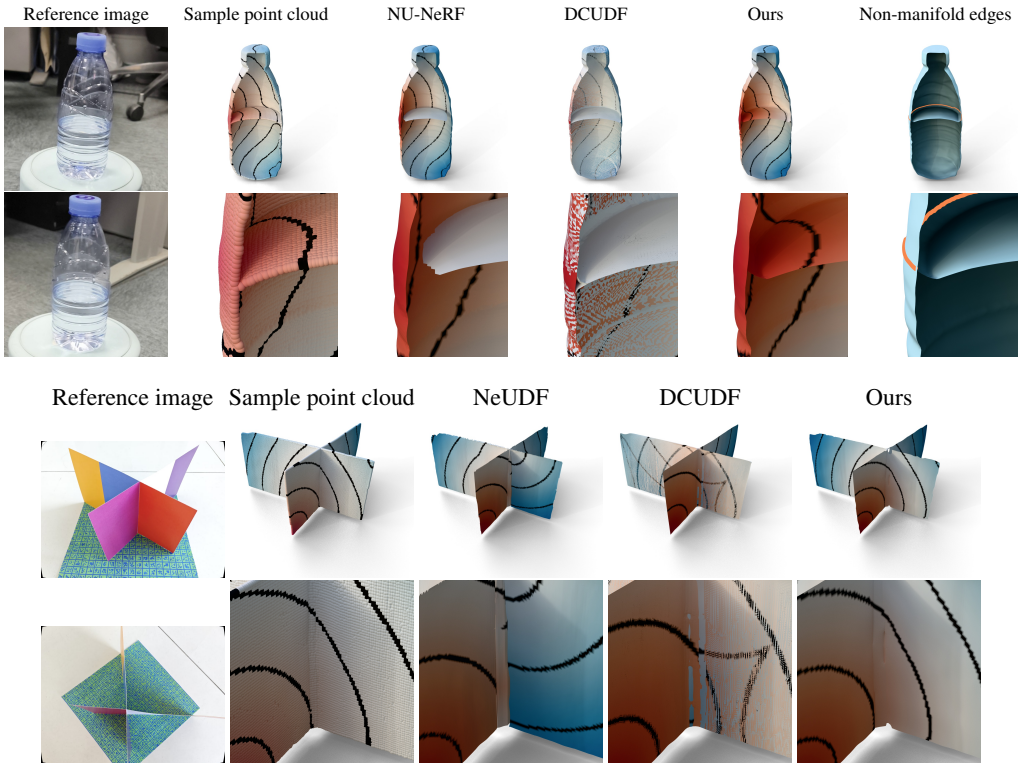

Figure 13: More results of Non-manifold surface extraction from SDFs/UDFs learned by NU-NeRF (top) and NeUDF (bottom). We use the SDFs provided directly by the NU-NeRF authors and convert them to UDFs.

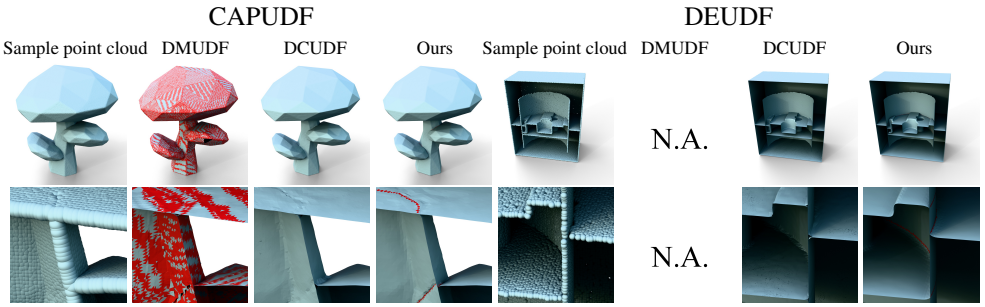

Figure 14: More results of non-manifold surface extraction from CAPUDF and DEUDF.

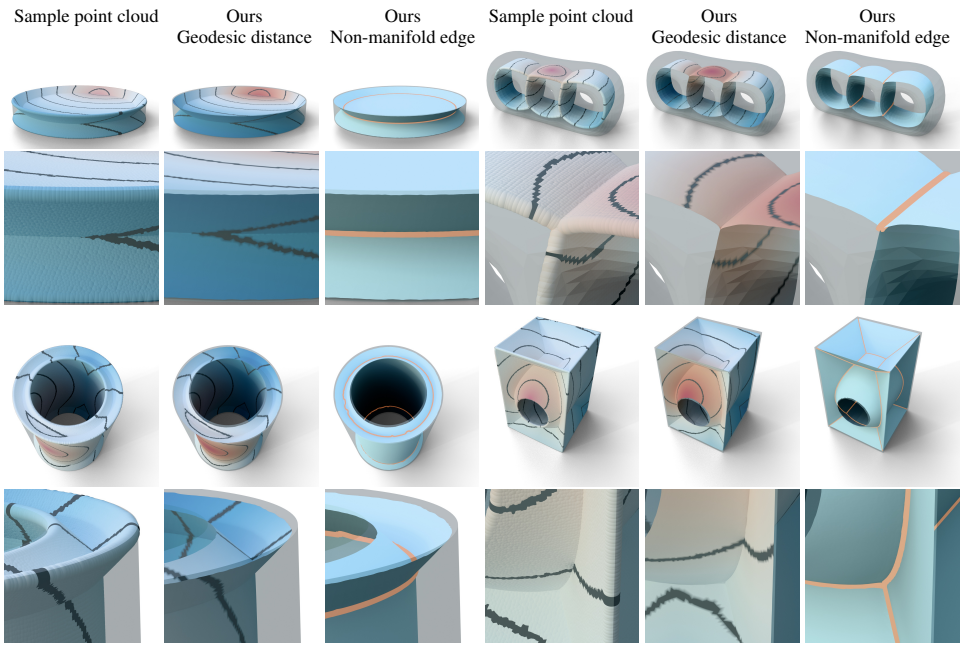

Figure 15: More results of non-manifold surface extraction from UDFs learned by Q-MDF [64].

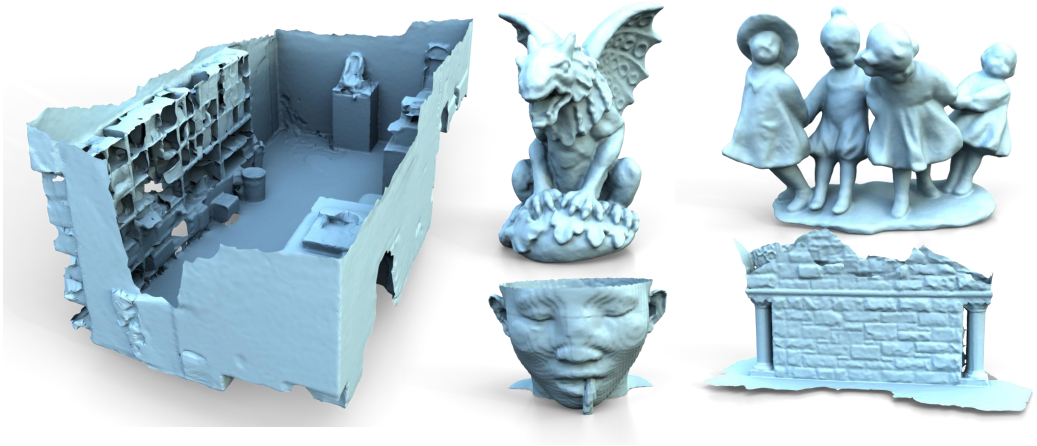

Figure 16: Results on more data, where the UDFs are learned by DEUDF [8]. We demonstrate the reconstruction results of indoor data, medical images, objects, and high fidelity surface data, which illustrates the applicability of our method.

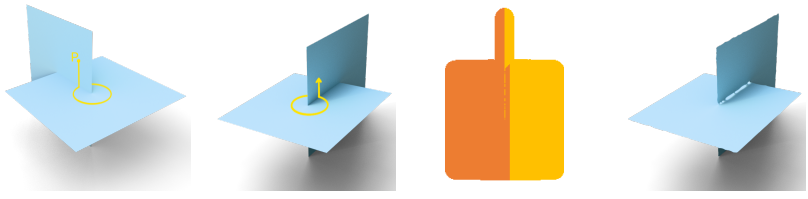

Figure 17: Non-orientable surfaces do not have proper MI definitions. (a) and (b) illustrate a non-orientable non-manifold surface where a walker can traverse from one side of a point to the opposite side without crossing a boundary. In such case, the multi-labeled field is undefined and thus fails to generate (c), from which the non-manifold surfaces cannot be extracted properly (d).

NeurIPS Paper Checklist

1. **Claims**

   Question: Do the main claims made in the abstract and introduction accurately reflect the paper's contributions and scope?

   Answer: [Yes]

   Justification: Our abstract and introduction 1 accurately reflect the paper's contributions and scope.

   Guidelines:

   - The answer NA means that the abstract and introduction do not include the claims made in the paper.
   - The abstract and/or introduction should clearly state the claims made, including the contributions made in the paper and important assumptions and limitations. A No or NA answer to this question will not be perceived well by the reviewers.
   - The claims made should match theoretical and experimental results, and reflect how much the results can be expected to generalize to other settings.
   - It is fine to include aspirational goals as motivation as long as it is clear that these goals are not attained by the paper.

2. **Limitations**

   Question: Does the paper discuss the limitations of the work performed by the authors?

   Answer: [Yes]

   Justification: We have a dedicated paragraph to discuss the limitations.

   Guidelines:

   - The answer NA means that the paper has no limitation while the answer No means that the paper has limitations, but those are not discussed in the paper.
   - The authors are encouraged to create a separate "Limitations" section in their paper.
   - The paper should point out any strong assumptions and how robust the results are to violations of these assumptions (e.g., independence assumptions, noiseless settings, model well-specification, asymptotic approximations only holding locally). The authors should reflect on how these assumptions might be violated in practice and what the implications would be.
   - The authors should reflect on the scope of the claims made, e.g., if the approach was only tested on a few datasets or with a few runs. In general, empirical results often depend on implicit assumptions, which should be articulated.
   - The authors should reflect on the factors that influence the performance of the approach. For example, a facial recognition algorithm may perform poorly when image resolution is low or images are taken in low lighting. Or a speech-to-text system might not be used reliably to provide closed captions for online lectures because it fails to handle technical jargon.
   - The authors should discuss the computational efficiency of the proposed algorithms and how they scale with dataset size.
   - If applicable, the authors should discuss possible limitations of their approach to address problems of privacy and fairness.
   - While the authors might fear that complete honesty about limitations might be used by reviewers as grounds for rejection, a worse outcome might be that reviewers discover limitations that aren't acknowledged in the paper. The authors should use their best judgment and recognize that individual actions in favor of transparency play an important role in developing norms that preserve the integrity of the community. Reviewers will be specifically instructed to not penalize honesty concerning limitations.

3. **Theory assumptions and proofs**

   Question: For each theoretical result, does the paper provide the full set of assumptions and a complete (and correct) proof?

   Answer: [NA]

Justification: Our paper does not include theoretical results.

Guidelines:

- The answer NA means that the paper does not include theoretical results.
- All the theorems, formulas, and proofs in the paper should be numbered and cross-referenced.
- All assumptions should be clearly stated or referenced in the statement of any theorems.
- The proofs can either appear in the main paper or the supplemental material, but if they appear in the supplemental material, the authors are encouraged to provide a short proof sketch to provide intuition.
- Inversely, any informal proof provided in the core of the paper should be complemented by formal proofs provided in appendix or supplemental material.
- Theorems and Lemmas that the proof relies upon should be properly referenced.

4. **Experimental result reproducibility**

   Question: Does the paper fully disclose all the information needed to reproduce the main experimental results of the paper to the extent that it affects the main claims and/or conclusions of the paper (regardless of whether the code and data are provided or not)?

   Answer: [Yes]

   Justification: All of our experimental results 4 are reproducible.

   Guidelines:

   - The answer NA means that the paper does not include experiments.
   - If the paper includes experiments, a No answer to this question will not be perceived well by the reviewers: Making the paper reproducible is important, regardless of whether the code and data are provided or not.
   - If the contribution is a dataset and/or model, the authors should describe the steps taken to make their results reproducible or verifiable.
   - Depending on the contribution, reproducibility can be accomplished in various ways. For example, if the contribution is a novel architecture, describing the architecture fully might suffice, or if the contribution is a specific model and empirical evaluation, it may be necessary to either make it possible for others to replicate the model with the same dataset, or provide access to the model. In general. releasing code and data is often one good way to accomplish this, but reproducibility can also be provided via detailed instructions for how to replicate the results, access to a hosted model (e.g., in the case of a large language model), releasing of a model checkpoint, or other means that are appropriate to the research performed.
   - While NeurIPS does not require releasing code, the conference does require all submissions to provide some reasonable avenue for reproducibility, which may depend on the nature of the contribution. For example
     (a) If the contribution is primarily a new algorithm, the paper should make it clear how to reproduce that algorithm.
     (b) If the contribution is primarily a new model architecture, the paper should describe the architecture clearly and fully.
     (c) If the contribution is a new model (e.g., a large language model), then there should either be a way to access this model for reproducing the results or a way to reproduce the model (e.g., with an open-source dataset or instructions for how to construct the dataset).
     (d) We recognize that reproducibility may be tricky in some cases, in which case authors are welcome to describe the particular way they provide for reproducibility. In the case of closed-source models, it may be that access to the model is limited in some way (e.g., to registered users), but it should be possible for other researchers to have some path to reproducing or verifying the results.

5. **Open access to data and code**

   Question: Does the paper provide open access to the data and code, with sufficient instructions to faithfully reproduce the main experimental results, as described in supplemental material?

Answer:[No]

Justification: We will open the source code and data after the acceptance of the paper.

Guidelines:

- The answer NA means that paper does not include experiments requiring code.
- Please see the NeurIPS code and data submission guidelines (`https://nips.cc/public/guides/CodeSubmissionPolicy`) for more details.
- While we encourage the release of code and data, we understand that this might not be possible, so "No" is an acceptable answer. Papers cannot be rejected simply for not including code, unless this is central to the contribution (e.g., for a new open-source benchmark).
- The instructions should contain the exact command and environment needed to run to reproduce the results. See the NeurIPS code and data submission guidelines (`https://nips.cc/public/guides/CodeSubmissionPolicy`) for more details.
- The authors should provide instructions on data access and preparation, including how to access the raw data, preprocessed data, intermediate data, and generated data, etc.
- The authors should provide scripts to reproduce all experimental results for the new proposed method and baselines. If only a subset of experiments are reproducible, they should state which ones are omitted from the script and why.
- At submission time, to preserve anonymity, the authors should release anonymized versions (if applicable).
- Providing as much information as possible in supplemental material (appended to the paper) is recommended, but including URLs to data and code is permitted.

6. **Experimental setting/details**

   Question: Does the paper specify all the training and test details (e.g., data splits, hyperparameters, how they were chosen, type of optimizer, etc.) necessary to understand the results?

   Answer: [Yes]

   Justification: Implementation details are introduced in Section 4.1

   Guidelines:

   - The answer NA means that the paper does not include experiments.
   - The experimental setting should be presented in the core of the paper to a level of detail that is necessary to appreciate the results and make sense of them.
   - The full details can be provided either with the code, in appendix, or as supplemental material.

7. **Experiment statistical significance**

   Question: Does the paper report error bars suitably and correctly defined or other appropriate information about the statistical significance of the experiments?

   Answer: [No]

   Justification: Like almost all methods, our input neural networks are randomly initialized. Our method does not depend on any special random numbers. We believe the different test cases in our experiments can explain the stability of our method.

   Guidelines:

   - The answer NA means that the paper does not include experiments.
   - The authors should answer "Yes" if the results are accompanied by error bars, confidence intervals, or statistical significance tests, at least for the experiments that support the main claims of the paper.
   - The factors of variability that the error bars are capturing should be clearly stated (for example, train/test split, initialization, random drawing of some parameter, or overall run with given experimental conditions).
   - The method for calculating the error bars should be explained (closed form formula, call to a library function, bootstrap, etc.)
   - The assumptions made should be given (e.g., Normally distributed errors).

- It should be clear whether the error bar is the standard deviation or the standard error of the mean.
- It is OK to report 1-sigma error bars, but one should state it. The authors should preferably report a 2-sigma error bar than state that they have a 96% CI, if the hypothesis of Normality of errors is not verified.
- For asymmetric distributions, the authors should be careful not to show in tables or figures symmetric error bars that would yield results that are out of range (e.g. negative error rates).
- If error bars are reported in tables or plots, The authors should explain in the text how they were calculated and reference the corresponding figures or tables in the text.

8. **Experiments compute resources**

   Question: For each experiment, does the paper provide sufficient information on the computer resources (type of compute workers, memory, time of execution) needed to reproduce the experiments?

   Answer: [Yes]

   Justification: Experiments Compute Resources are introduced in Section 4.1

   Guidelines:

   - The answer NA means that the paper does not include experiments.
   - The paper should indicate the type of compute workers CPU or GPU, internal cluster, or cloud provider, including relevant memory and storage.
   - The paper should provide the amount of compute required for each of the individual experimental runs as well as estimate the total compute.
   - The paper should disclose whether the full research project required more compute than the experiments reported in the paper (e.g., preliminary or failed experiments that didn't make it into the paper).

9. **Code of ethics**

   Question: Does the research conducted in the paper conform, in every respect, with the NeurIPS Code of Ethics `https://neurips.cc/public/EthicsGuidelines`?

   Answer: [Yes]

   Justification: The research conducted in the paper fully conforms to the NeurIPS Code of Ethics.

   Guidelines:

   - The answer NA means that the authors have not reviewed the NeurIPS Code of Ethics.
   - If the authors answer No, they should explain the special circumstances that require a deviation from the Code of Ethics.
   - The authors should make sure to preserve anonymity (e.g., if there is a special consideration due to laws or regulations in their jurisdiction).

10. **Broader impacts**

    Question: Does the paper discuss both potential positive societal impacts and negative societal impacts of the work performed?

    Answer: [NA]

    Justification: To the best of our imagination we cannot think of potential misuse of our proposed approach that leaves a negative impact to the society.

    Guidelines:

    - The answer NA means that there is no societal impact of the work performed.
    - If the authors answer NA or No, they should explain why their work has no societal impact or why the paper does not address societal impact.
    - Examples of negative societal impacts include potential malicious or unintended uses (e.g., disinformation, generating fake profiles, surveillance), fairness considerations (e.g., deployment of technologies that could make decisions that unfairly impact specific groups), privacy considerations, and security considerations.

- The conference expects that many papers will be foundational research and not tied to particular applications, let alone deployments. However, if there is a direct path to any negative applications, the authors should point it out. For example, it is legitimate to point out that an improvement in the quality of generative models could be used to generate deepfakes for disinformation. On the other hand, it is not needed to point out that a generic algorithm for optimizing neural networks could enable people to train models that generate Deepfakes faster.
- The authors should consider possible harms that could arise when the technology is being used as intended and functioning correctly, harms that could arise when the technology is being used as intended but gives incorrect results, and harms following from (intentional or unintentional) misuse of the technology.
- If there are negative societal impacts, the authors could also discuss possible mitigation strategies (e.g., gated release of models, providing defenses in addition to attacks, mechanisms for monitoring misuse, mechanisms to monitor how a system learns from feedback over time, improving the efficiency and accessibility of ML).

11. **Safeguards**

    Question: Does the paper describe safeguards that have been put in place for responsible release of data or models that have a high risk for misuse (e.g., pretrained language models, image generators, or scraped datasets)?

    Answer: [NA]

    Justification: This paper does not pose such risks.

    Guidelines:

    - The answer NA means that the paper poses no such risks.
    - Released models that have a high risk for misuse or dual-use should be released with necessary safeguards to allow for controlled use of the model, for example by requiring that users adhere to usage guidelines or restrictions to access the model or implementing safety filters.
    - Datasets that have been scraped from the Internet could pose safety risks. The authors should describe how they avoided releasing unsafe images.
    - We recognize that providing effective safeguards is challenging, and many papers do not require this, but we encourage authors to take this into account and make a best faith effort.

12. **Licenses for existing assets**

    Question: Are the creators or original owners of assets (e.g., code, data, models), used in the paper, properly credited and are the license and terms of use explicitly mentioned and properly respected?

    Answer: [Yes]

    Justification: The creators or original owners of assets (e.g., code, data, models), used in the paper, are properly credited and the license and terms of use are explicitly mentioned and properly respected.

    Guidelines:

    - The answer NA means that the paper does not use existing assets.
    - The authors should cite the original paper that produced the code package or dataset.
    - The authors should state which version of the asset is used and, if possible, include a URL.
    - The name of the license (e.g., CC-BY 4.0) should be included for each asset.
    - For scraped data from a particular source (e.g., website), the copyright and terms of service of that source should be provided.
    - If assets are released, the license, copyright information, and terms of use in the package should be provided. For popular datasets, `paperswithcode.com/datasets` has curated licenses for some datasets. Their licensing guide can help determine the license of a dataset.

- For existing datasets that are re-packaged, both the original license and the license of the derived asset (if it has changed) should be provided.
- If this information is not available online, the authors are encouraged to reach out to the asset's creators.

13. **New assets**

    Question: Are new assets introduced in the paper well documented and is the documentation provided alongside the assets?

    Answer: [NA]

    Justification: The paper does not release new assets.

    Guidelines:

    - The answer NA means that the paper does not release new assets.
    - Researchers should communicate the details of the dataset/code/model as part of their submissions via structured templates. This includes details about training, license, limitations, etc.
    - The paper should discuss whether and how consent was obtained from people whose asset is used.
    - At submission time, remember to anonymize your assets (if applicable). You can either create an anonymized URL or include an anonymized zip file.

14. **Crowdsourcing and research with human subjects**

    Question: For crowdsourcing experiments and research with human subjects, does the paper include the full text of instructions given to participants and screenshots, if applicable, as well as details about compensation (if any)?

    Answer: [NA]

    Justification: The paper does not involve crowdsourcing nor research with human subjects.

    Guidelines:

    - The answer NA means that the paper does not involve crowdsourcing nor research with human subjects.
    - Including this information in the supplemental material is fine, but if the main contribution of the paper involves human subjects, then as much detail as possible should be included in the main paper.
    - According to the NeurIPS Code of Ethics, workers involved in data collection, curation, or other labor should be paid at least the minimum wage in the country of the data collector.

15. **Institutional review board (IRB) approvals or equivalent for research with human subjects**

    Question: Does the paper describe potential risks incurred by study participants, whether such risks were disclosed to the subjects, and whether Institutional Review Board (IRB) approvals (or an equivalent approval/review based on the requirements of your country or institution) were obtained?

    Answer: [NA]

    Justification: The paper does not involve crowdsourcing nor research with human subjects.

    Guidelines:

    - The answer NA means that the paper does not involve crowdsourcing nor research with human subjects.
    - Depending on the country in which research is conducted, IRB approval (or equivalent) may be required for any human subjects research. If you obtained IRB approval, you should clearly state this in the paper.
    - We recognize that the procedures for this may vary significantly between institutions and locations, and we expect authors to adhere to the NeurIPS Code of Ethics and the guidelines for their institution.
    - For initial submissions, do not include any information that would break anonymity (if applicable), such as the institution conducting the review.

16. **Declaration of LLM usage**

Question: Does the paper describe the usage of LLMs if it is an important, original, or non-standard component of the core methods in this research? Note that if the LLM is used only for writing, editing, or formatting purposes and does not impact the core methodology, scientific rigorousness, or originality of the research, declaration is not required.

Answer: [NA]

Justification: LLMs were used solely for grammar correction and writing refinement.

Guidelines:

- The answer NA means that the core method development in this research does not involve LLMs as any important, original, or non-standard components.
- Please refer to our LLM policy (`https://neurips.cc/Conferences/2025/LLM`) for what should or should not be described.